

Anomalous H/D Isotope Effect on ^{35}Cl NQR Frequencies and H/D Isotope Effect on ^{1}H MAS NMR Spectra in Pyrrolidinium *p*-Chlorobenzoate

Ryo Nakano,[1] Hisashi Honda,*[1,2,3] Taiki Kimura,[2] Shin-shin Kyo,[2] Shin'ichi Ishimaru,[4] Ryosuke Miyake,[3] Eiichi Nakata,[1] Satoshi Takamizawa,[1,2,3] and Sumiko Noro[1,2]

[1]Graduate School of Integrated Science, Yokohama City University, Kanazawa-ku, Yokohama 236-0027

[2]Faculty of Science, Yokohama City University, Kanazawa-ku, Yokohama 236-0027

[3]Graduate School of Nanobioscience, Yokohama City University, Kanazawa-ku, Yokohama 236-0027

[4]Department of Green and Sustainable Chemistry, Tokyo Denki University, Chiyoda-ku, Tokyo 101-8457

Received November 19, 2009; E-mail: hhonda@yokohama-cu.ac.jp

An anomalous isotope effect was observed in the ^{35}Cl NQR frequency of pyrrolidinium *p*-chlorobenzoate ($C_4H_8NH_2^+ \cdot ClC_6H_4COO^-$) by deuterium substitution of hydrogen atoms which form two kinds of N–H···O type hydrogen bonds. Large negative frequency shifts of the ^{35}Cl resonance lines, reaching 309 kHz at 77 K and 267 kHz at 293 K, were obtained upon deuteration, although the Cl atom in the molecule formed no hydrogen bonds in the crystal. ^{1}H MAS NMR lines showed significant changes by the deuterium substitution, while in contrast, small shifts of ^{13}C CP/MAS NMR signals were obtained. Our measurements of ^{1}H NMR spin–lattice relaxation times (T_1) suggested that the H/D isotope shifts detected from the ^{35}Cl NQR frequencies and ^{1}H NMR spectra are due to structural changes rather than molecular dynamics. Single-crystal X-ray diffraction measurements showed two remarkable H/D isotope differences in the molecular arrangements, (i) the N–H length along the crystallographic *a* axis became 1 pm shorter, and (ii) the dihedral angle between benzene and the pyrrolidine ring changed by 1.1(2)° upon deuteration. Using density functional theory estimations, the anomalous ^{35}Cl NQR frequency shifts and ^{1}H MAS NMR line-shape changes could be explained by the dihedral angle change rather than the N–H length difference.

X-ray diffraction measurements have revealed that substitution of H atoms, forming hydrogen bonds (A–H···B), with D atoms results in A···B length changes.[1–4] Determining the accurate position of H atoms, however, has been difficult by X-ray diffraction measurements. Nuclear quadrupole resonance (NQR) methods have often been employed to study H/D isotope effects because NQR frequencies (ν_Q) can be detected even with very small changes in the electronic environment around the observed atoms. After deuterium substitution, ^{35}Cl NQR measurements have shown frequency shifts of dozens of kHz for covalently-attached Cl atoms and up to several hundred kHz (occasionally reaching MHz order) for ionic Cl^- atoms.[5–16] However, there have been few reports of large H/D isotope effects on NQR frequencies of Cl atoms that form non-hydrogen bonds without significant structural changes.[17] Nuclear magnetic resonance (NMR) measurements have sometimes been used to detect electron density changes in ^{13}C atoms. ^{13}C cross polarization (CP) and magic-angle-spinning (MAS) NMR peaks however show shifts of a few ppm by deuteration.[18–22] High-resolution ^{1}H NMR signals obtained in solid states has been difficult, because of very large dipole–dipole interactions among ^{1}H nuclei, except in special cases. High-speed MAS techniques have recently allowed us to record high-resolution ^{1}H MAS NMR spectra for solid samples.

We have reported anomalous H/D isotope effects on ^{35}Cl NQR frequency of piperidinium *p*-chlorobenzoate ($C_5H_{10}NH_2^+ \cdot ClC_6H_4COO^-$), revealing a dihedral angle change of 1.8° between the benzene and piperidine ring contributing to large frequency shifts of ca. 280 kHz.[17] Pyrrolidinium *p*-chlorobenzoate ($C_4H_8NH_2^+ \cdot ClC_6H_4COO^-$, abbreviated to PYC(H)) crystals show similar molecular arrangements as in piperidinium *p*-chlorobenzoate crystals: each molecule is linked by two types of hydrogen bonds (N–H···O) and the crystal belongs to the space group of *Pbca*.[23,24] These facts predict that anomalous H/D isotope effects on ^{35}Cl NQR frequencies can also be detected in PYC(H). In addition, our results of single-crystal X-ray diffraction observations in piperidinium *p*-chlorobenzoate showed not only a dihedral angle change but also N–H length shortening by deuterium substitution.

Based upon the foregoing, we carried out not only ^{35}Cl NQR frequency and single-crystal X-ray diffraction investigations but also determined ^{1}H MAS NMR, ^{2}H NMR, and ^{13}C CP/MAS NMR spectra to detect H/D isotope effects on electron states of each atom in the crystal. Moreover, ^{1}H NMR spin–lattice relaxation time, T_1, measurements were performed for both PYC(H) and pyrrolidinium *p*-chlorobenzoate-d_2 ($C_4H_8ND_2^+ \cdot ClC_6H_4COO^-$, abbreviated to PYC(D)) to get information on dynamical H/D isotope changes. Here, we

Published on the web September 2, 2010; doi:10.1246/bcsj.20090300

employ the symbols H-bond(*a*) and H-bond(*b*), respectively, for hydrogen bonds along crystallographic *a*- and *b* axis.

Experimental

PYC(H) crystals were prepared by adding pyrrolidine to a hot benzene solution of *p*-chlorobenzoic acid and by evaporating the solvent. The crude specimens obtained were recrystallized from benzene in a dessicator with $CaCl_2$ as the drying agent. PYC(D) was prepared by crystallizing three times from a hot CH_3OD (99% deuterated, Cambridge Isotope Laboratories, Inc.) and recrystallization from dried benzene in a dessicator with $CaCl_2$, where all manipulations were carried out under dry N_2 gas.

Measurements of ^{35}Cl NQR frequency were performed using a handmade Dean-type super-regenerative spectrometer. The samples were sealed in Pyrex sample tubes with an outer diameter of 12 mm. The NQR signals obtained were amplified by a Lock-in-amplifier (NF Corp.) and registered using a pen recorder. The sample temperature was obtained using a thermocouple with an accuracy of ± 1 K. The estimated uncertainty in the frequency was 1 kHz.

Solid-state high-resolution ^{1}H NMR experiments were carried out at a Larmor frequency of 600.13 MHz with a Bruker Avance 600 spectrometer with a MAS accessory. The samples were packed in a ZrO rotor with an outer diameter of 2.5 mm and the spinning rate was kept at 35 kHz through the acquisition of FID. Spectra were obtained from FID signals which were obtained after a $\pi/2$ pulse. We chose a recycle time of 600 s for PYC(H) and PYC(D). ^{1}H chemical shifts (CS) were calibrated relative to an external adamantane (1.91 ppm) reference.

^{1}H NMR T_1 measurements were performed at a Larmor Frequency of 40.0 MHz using a Bruker SXP spectrometer in the temperature range from 90 K to room temperature. The sample temperature was recorded employing a thermocouple with an accuracy of ± 1 K. The saturation recovery method was introduced for the determination of T_1 in the whole temperature range studied.

The ^{2}H NMR spectrum was recorded at a Larmor frequency of 46.07 MHz using a Bruker MSL-300 spectrometer. The PYC(D) powder sample was placed in a Pyrex tube with an outer diameter of 5 mm. The spectrum was obtained from echo signals after a $(\pi/2)_x - \tau - (\pi/2)_y - \tau$ pulse sequence with a recycle delay of 1000 s.

^{13}C CP/MAS NMR spectra measurements were carried out at a Larmor frequency of 150.9 MHz with a Bruker Avance 600 spectrometer. We packed the sample in a rotor with an outer diameter of 4.0 mm ZrO rotor and recorded spectra for three spinning rates of 5, 7, and 12 kHz, to distinguish signals from spinning side bands. A ramp pulse sequence[25] was employed for recording the spectra with a spinning rate of 12 kHz. The CS of the ^{13}C nuclei was calibrated by an external adamantane (29.47 ppm) reference. CP/MAS spectra were recorded with a contact time of 1.0 ms.

Single-crystal X-ray analysis was performed on a Bruker Smart APEX CCD area diffractometer using graphite-monochromated Mo Kα radiation ($\lambda = 71.073$ pm). Empirical absorption corrections were applied using the SADABS program.[26] The structures were solved by a direct method (SHELXS-97)[27] and refined by full-matrix least-squares calculations on F^2 (SHELXL-97) employing the SHELX-TL program package. Non-hydrogen atoms were refined anisotropically and hydrogen atoms were refined isotropically. Crystal sizes of $0.45 \times 0.40 \times 0.30$ mm^3 for PYC(D) and $0.42 \times 0.35 \times 0.31$ mm^3 for PYC(H) were employed. Crystallographic data have been deposited with Cambridge Crystallographic Data Centre: Deposition number CCDC-778349 and -778350, respectively, for PYC(D) and PYC(H). Copies of the data can be obtained free of charge via http://www.ccdc.cam.ac.uk/conts/retrieving.html (or from the Cambridge Crystallographic Data Centre, 12, Union Road, Cambridge, CB2 1EZ, U.K.; Fax: +44 1223 336033; e-mail: deposit@ccdc.cam.ac.uk).

Density functional theory (DFT) calculations were carried out using the Gaussian 03w computer program[28] to estimate the potential curve, theoretical values of electric-field gradient (EFG) at ^{2}H and ^{35}Cl atoms, and shielding tensor of the ^{1}H and ^{13}C nuclei. All calculations were performed using the crystal parameters obtained from our single-crystal X-ray measurements of PYC(H) and PYC(D).

Results and Discussion

X-ray Diffraction and Melting Point. The lattice constants and the crystallographic data obtained at 90 K for PYC(H) and PYC(D) are listed respectively in Tables 1 and 2, and the crystal structure observed for PYC(H) are shown in Figure 1.[29] The parameters obtained for the PYC(H) crystal were almost the same as those reported previously, however, the *R*-value of 0.0439 recorded in the present work was much smaller than the reported value of 0.141.[24] The crystal data obtained in PYC(D) (*R*-value of 0.0375) were nearly identical to those of PYC(H) without a few differences described the following. One is the N–H length; a little changes of the distance along the H-bond(*a*) and H-bond(*b*) was observed, as shown in Table 3. Another significant structural difference by deuterium substitution is the dihedral angle between benzene and pyrrolidine rings; the angle was changed by 1.1(2)°. Here, pyrrolidine ring formed a twisted structure as displayed in Figure 1, therefore the dihedral angle between benzene ring and a plane formed by C(8), N(13), and C(11) atoms in pyrrolidine was measured. In this study, the dihedral angle between benzene and pyrrolidine ring means this angle. The isotope changes of 1.1° was similar to reported values in piperidinium *p*-chlorobenzoate crystals.[17]

The difference in the melting point (424.0 K for PYC(H) and 416.5 K for PYC(D)) was also similar to that for piperidinium *p*-chlorobenzoate crystals (414.5 (H) and 404.5 K (D)).[17]

^{35}Cl NQR Frequency. One ^{35}Cl NQR signal was observed in the temperature range from 77 K to the melting point for each PYC(H) and PYC(D) crystal, as shown in Figure 2. This result is consistent with the crystal structure in which there is only one Cl site in both crystals. The obtained frequencies of 34.327 (PYC(H)) and 34.018 MHz (PYC(D)) at 77 K were successively decreased (to 33.672 MHz for PYC(H) and 33.405 MHz for PYC(D) at 293 K) with increasing temperature. The frequency difference ($\Delta\nu_Q$) gradually reduced with temperature, however, large shifts were detected up to the melting temperature. The recorded large isotope shifts of the ^{35}Cl NQR

Table 1. Crystallographic Data and Structure Refinement of Pyrrolidinium *p*-Chlorobenzoate (PYC(H)) and of Pyrrolidinium *p*-Chlorobenzoate-d_2 (PYC(D))

	Pyrrolidinium *p*-chlorobenzoate PYC(H)	Pyrrolidinium *p*-chlorobenzoate-d_2 PYC(D)
Empirical formula	$C_{11}H_{14}ClNO_2$	$C_{11}H_{12}ClD_2NO_2$
Formula weight	227.68	229.69
Crystal system	Orthorhombic	Orthorhombic
Space group	*Pbca*	*Pbca*
Unit cell dimensions/nm	$a = 0.91404(5)$	$a = 0.91555(5)$
	$b = 2.65952(16)$	$b = 2.66266(14)$
	$c = 0.94202(6)$	$c = 0.94198(5)$
Volume/nm^3	2.2900(2)	2.2964(2)
Z	8	8
Density (calculated)/Mg m^{-3}	1.321	1.329
Absorption coefficient/mm^{-1}	0.314	0.313
F(000)	960	960
Crystal size/mm^3	$0.42 \times 0.35 \times 0.31$	$0.45 \times 0.40 \times 0.30$
θ range for data collection	1.53 to 28.30°	2.65 to 28.31°
Index ranges	$-12 \leqq h \leqq 8$, $-34 \leqq k \leqq 35$, $-10 \leqq l \leqq 12$	$-12 \leqq h \leqq 11$, $-25 \leqq k \leqq 35$, $-10 \leqq l \leqq 12$
Reflections collected	15833	15978
Independent reflections	2851 [$R_{int} = 0.0468$]	2857 [$R_{int} = 0.0370$]
Max. and min. transmission	0.9090 and 0.8795	0.9120 and 0.8721
Refinement method	Full-matrix least-squares on F^2	Full-matrix least-squares on F^2
Data/restraints/parameters	2851/0/192	2857/0/192
Goodness-of-fit on F^2	1.075	1.022
Final R indices [$I > 2\sigma(I)$]	$R1 = 0.0439$, $wR2 = 0.1044$	$R1 = 0.0375$, $wR2 = 0.0898$
R indices (all data)	$R1 = 0.0605$, $wR2 = 0.1202$	$R1 = 0.0496$, $wR2 = 0.0965$
Largest diff. peak and hole	0.418 and -0.218 e Å^{-3}	0.322 and -0.201 e Å^{-3}

Table 2. Bond Lengths/pm and Angles/° of Pyrrolidinium *p*-Chlorobenzoate (PYC(H)) and of Pyrrolidinium *p*-Chlorobenzoate-d_2 (PYC(D))

	PYC(H)	PYC(D)
Intramolecular		
C(1)–C(2)	138.0(3)	138.0(2)
C(2)–C(3)	138.7(3)	139.0(2)
C(3)–C(4)	139.1(2)	138.85(19)
C(4)–C(5)	139.1(2)	139.26(18)
C(5)–C(6)	138.3(3)	138.6(2)
C(1)–C(6)	137.8(3)	138.1(2)
C(1)–Cl(12)	174.32(18)	174.36(15)
C(4)–C(7)	150.8(2)	151.31(18)
C(7)–O(14)	125.3(2)	125.38(16)
C(7)–O(15)	126.2(2)	126.06(16)
C(8)–N(13)	149.8(2)	149.77(17)
C(8)–C(9)	150.6(3)	150.8(2)
C(9)–C(10)	151.5(3)	151.8(2)
C(10)–C(11)	152.1(3)	152.3(2)
C(11)–N(13)	150.1(2)	150.45(18)
C(2)–H(18)	97(2)	96.4(17)
C(3)–H(19)	93(2)	97.1(16)
C(5)–H(20)	93.6(19)	96.2(17)
C(6)–H(21)	92(2)	93.7(18)
C(8)–H(22)	97(2)	96.3(17)
C(8)–H(26)	96(2)	96.6(19)
C(9)–H(23)	105(2)	101.7(18)
C(9)–H(27)	107(3)	101(2)
C(10)–H(24)	93(3)	97(2)
C(10)–H(28)	106(3)	97(2)
C(11)–H(25)	93(2)	97.8(18)
C(11)–H(29)	102(2)	96.6(17)
C(2)–C(1)–C(6)	122.08(17)	121.91(14)
C(6)–C(1)–Cl(12)	119.48(14)	119.52(12)
C(2)–C(1)–Cl(12)	118.44(14)	118.57(12)
C(1)–C(2)–H(18)	118.1(12)	119.2(10)
C(3)–C(2)–H(18)	123.1(12)	121.8(10)
C(2)–C(3)–H(19)	116.1(13)	119.6(10)
C(4)–C(3)–H(19)	123.3(13)	120.0(10)
C(3)–C(4)–C(5)	118.89(16)	119.29(12)
C(3)–C(4)–C(7)	120.84(15)	120.91(12)
C(5)–C(4)–C(7)	120.26(15)	119.80(12)
C(4)–C(5)–H(20)	121.0(12)	119.0(10)
C(1)–C(6)–H(21)	121.7(13)	121.3(10)
C(5)–C(6)–H(21)	119.9(13)	120.2(11)
O(14)–C(7)–O(15)	124.68(16)	124.88(12)
O(14)–C(7)–C(4)	118.92(14)	118.51(12)
O(15)–C(7)–C(4)	116.39(14)	116.60(11)
H(22)–C(8)–H(26)	111.2(17)	109.0(14)
N(13)–C(8)–H(22)	108.4(12)	108.3(10)
N(13)–C(8)–H(26)	109.5(13)	107.7(11)
N(13)–C(8)–C(9)	103.77(14)	103.65(11)
H(27)–C(9)–H(23)	103.7(18)	107.0(15)
C(8)–C(9)–C(10)	102.41(16)	102.47(13)
H(28)–C(10)–H(24)	107(2)	108.2(17)
C(9)–C(10)–C(11)	104.30(16)	104.30(13)
H(29)–C(11)–H(25)	111.5(18)	111.9(14)
N(13)–C(11)–H(25)	109.7(14)	108.0(10)
N(13)–C(11)–H(29)	108.7(12)	105.7(10)
N(13)–C(11)–C(10)	105.01(14)	104.87(11)
C(8)–N(13)–C(11)	107.85(14)	108.01(11)
Intermolecular		
Cl(12)···C(6)	382.1(1)	383.2(1)
Cl(12)···C(10)	388.0(1)	385.3(1)
Cl(12)···H(21)	334(1)	335(1)
Cl(12)···H(28)	291(1)	292(1)

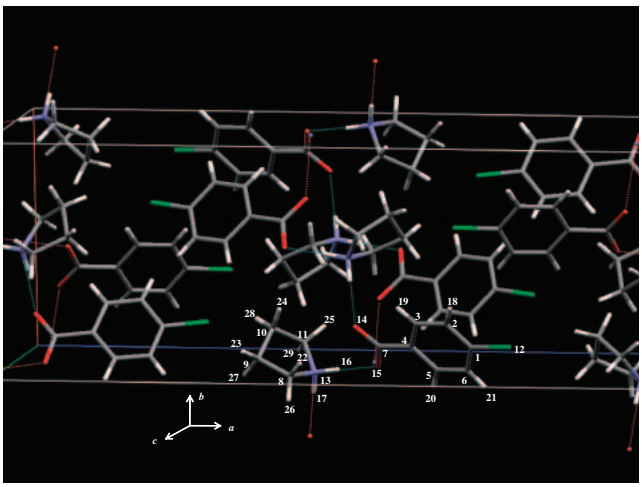

Figure 1. Crystal structure of pyrrolidinium *p*-chlorobenzoate. Dashed lines indicate N–H···O hydrogen bonds.

Table 3. Observed Bond Lengths/pm and Hydrogen Bond Angles/°

		d(N–H)	*d*(H···O)	*d*(N···O)	∠(NHO)
N–H···O	H-bond(*a*)	95(2)	172(2)	266.95(15)	177.3(18)
N–H···O	H-bond(*b*)	92.2(19)	182(2)	272.63(15)	165.7(16)
N–D···O	H-bond(*a*)	94(2)	173(2)	266.99(18)	175.7(20)
N–D···O	H-bond(*b*)	93.2(20)	181(2)	273.12(19)	166.4(19)

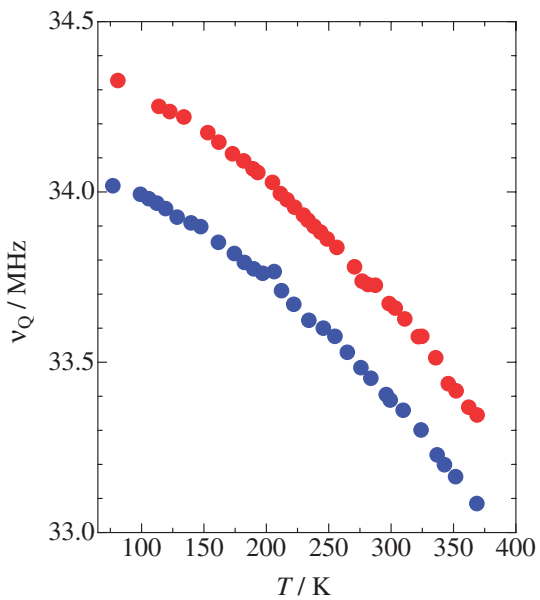

Figure 2. Temperature dependence of the ^{35}Cl NQR frequency (ν_Q) for pyrrolidinium *p*-chlorobenzoate (PYC(H)) (●) and pyrrolidinium *p*-chlorobenzoate-d_2 (PYC(D)) (●).

frequency are comparable to those of piperidinium *p*-chlorobenzoate crystals (278 kHz at 293 K).[17] These anomalous large shifts which are comparable to those of ionic Cl atoms forming Cl^-···H–O type hydrogen bonds, have been rarely reported for covalently-bonded Cl atoms without forming hydrogen bonds in the crystals.[5–17]

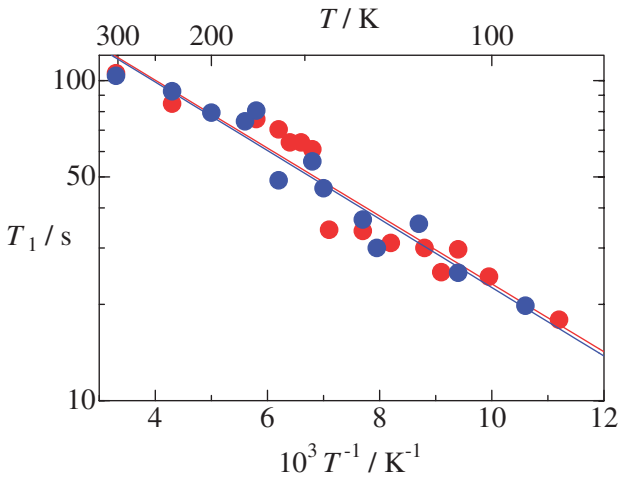

Figure 3. Temperature dependence of ^{1}H NMR spin–lattice relaxation times (T_1) observed at 40.0 MHz in pyrrolidinium *p*-chlorobenzoate (PYC(H)) (●) and pyrrolidinium *p*-chlorobenzoate-d_2 (PYC(D)) (●). The solid lines of (▬) and (▬) represent best-fit theoretical values for PYC(H) and PYC(D), respectively.

The X-ray diffraction data obtained from PYC(H) and PYC(D) crystals yielded the same space group and the almost the same lattice constants as listed in Tables 1 and 2, therefore, some assumptions of small atomic rearrangements or/and modulations of molecular motions affecting the anomalous isotope shifts of ^{35}Cl NQR frequencies can be introduced. In order to estimate contribution of molecular motions for the NQR frequency, we measured the ^{1}H NMR spin lattice relaxation time (T_1) for both samples.

^{1}H NMR T_1. The magnetic recovery curves obtained could be fitted to a single exponential component for all observed temperatures. A ^{1}H NMR T_1 value for each temperature was estimated from the slope of the magnetic recovery curves. T_1 values of PYC(H) and PYC(D) increased with temperature, as displayed in Figure 3. Assuming Arrhenius-type function, the T_1 slope showed an activation energy of 46 kJ mol^{-1} for PYC(H) and PYC(D) crystals. If some molecular motion which modulates dipole–dipole interaction among ^{1}H nuclei contributes to the relaxation, the slopes obtained with negative sign and large activation energies suggest that there are fast molecular motions which go over a large activation barrier in the crystal. The motional modes, however, could not be uniquely determined, because no disorder in the atomic position was recorded in our single-crystal X-ray diffraction measurements. Another mechanism contributing to the T_1 process can be assumed. Since the observed NMR frequency of 40 MHz is similar to ^{35}Cl NQR frequencies of ca. 34 MHz which increased with decreasing temperature and quadrupole relaxation rates are generally faster than dipole–dipole relaxation, it is considerable that ^{35}Cl nuclear relaxation modulates local magnetic fields at ^{1}H nuclei. Other effects contributing to the ^{1}H T_1 process are considerable, however, we are interested in the result that similar T_1 values were obtained in PYC(H) and PYC(D), therefore more detail discussion was not described in this literature. Based on the result of similar temperature dependence of T_1 values between PYC(H) and PYC(D)

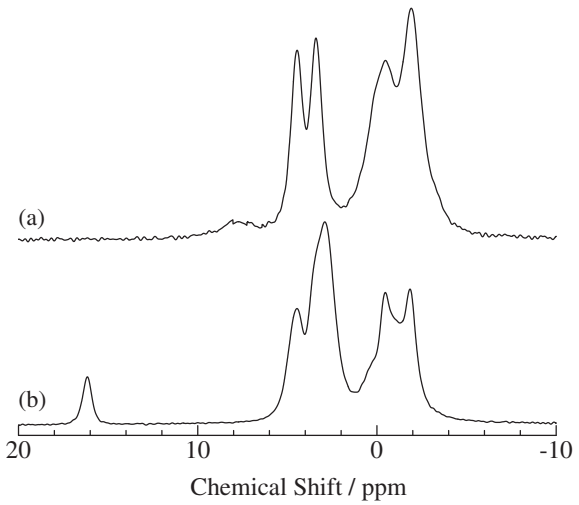

Figure 4. ^{1}H MAS NMR spectra of (a) pyrrolidinium *p*-chlorobenzoate (PYC(H)) and (b) pyrrolidinium *p*-chlorobenzoate-d_2 (PYC(D)) crystals.

crystals, we can consider that H/D isotope substitution contributes to static rearrangements in the crystals rather than dynamical changes of molecular motions.

^{1}H MAS NMR Spectra. ^{1}H MAS NMR spectra observed in PYC(H) and PYC(D) are shown in Figure 4. The PYC(H) and PYC(D) lines were recorded with a MAS speed of 35 kHz and recycle time of 600 s. In order to assign the peaks, ^{1}H NMR measurements of PYC(H) in a benzene solution and shielding tensor calculation with a B3LYP/6-311+G(3df,3pd) function were carried out. The obtained and assigned CS values are listed in Table 4. On the basis of the values in Table 4, signals recorded on −2 to 1.5 ppm and 2.5 to 5 ppm are assignable respectively to ^{1}H atoms bonding to pyrrolidine and to the benzene ring. The peak observed at 16.1 ppm is explainable to the ^{1}H atom in H-bond(*a*). The signal of the ^{1}H atom in the H-bond(*b*) would be observed around −1 ppm, because our DFT estimation showed a peak of −0.88 ppm. Since this value is similar to ^{1}H CS of pyrrolidine, the peak of the ^{1}H atom in H-bond(*b*) could not be distinguished on the spectrum. In order to assign observed ^{1}H CS values in the crystal, we introduced 14 Gauss functions where we assumed the same line-width of all H atoms bonded to C atoms of benzene and pyrrolidine ring. Simulated line-shapes are shown in Figure 5.

By the isotope substitution, two significant changes were detected in the spectra, i) the peak at 16.1 ppm, assigned to the H atom in H-bond(*a*), disappeared, and ii) line widths of two signals around 6 and −1 ppm of PYC(H) were changed, especially, the peak around 3 ppm became narrow in PYC(D). The former result guarantees that a high ratio of deuterium substitution was achieved. The latter result has been rarely reported in ^{1}H NMR spectra in solids. In order to reveal the origins of the recorded isotope changes of the ^{1}H MAS NMR spectrum, DFT calculations were performed for CS estimations. The data obtained and detailed discussions are described in the section: **DFT Calculation**.

^{13}C CP/MAS NMR. ^{13}C CP/MAS NMR spectra obtained at room temperature for PYC(H) and PYC(D) are shown in Figure 6. Using three spinning rates (5, 7, and 12 kHz), we could separate the signals and the spinning-side-band (SSB) peaks. Each peak could be assigned using the results of the ^{13}C NMR spectrum observed in the benzene solution

Table 4. ^{1}H and ^{13}C Chemical Shifts in ppm Observed for Pyrrolidinium *p*-Chlorobenzoate Crystals and in Benzene, and Estimated by a B3LYP/6-311+G(3df,3pd) Function

Atom	Observed CS in crystal		Observed CS in benzene	Calculated CS
	PYC(H)	PYC(D)		
C(1)	136.05	136.02	134.84	146.35
C(2)	128.22	128.91	128.69	124.36
C(3)	134.53	134.37	131.35	133.98
C(4)	131.32	131.30	129.71	143.82
C(5)	134.53	134.37	131.35	133.01
C(6)	128.22	128.91	128.69	126.86
C(7)	171.88	171.81	166.50	179.33
C(8)	43.97	43.87	47.22	34.07
C(9)	24.66	24.72	25.66	13.07
C(10)	24.66	24.72	25.66	15.30
C(11)	43.97	43.87	47.22	36.23
H(16)	16.1	—	3.64	12.88
H(17)			3.64	−0.88
H(18)	2.5–3.5	3–3.5	8.28	4.73
H(19)	4.5	4.5	7.28	6.81
H(20)	2.5–3.5		7.28	6.68
H(21)			8.28	5.26
H(22)	−2–−1.5	−2.5–−1.5	1.28	−1.35
H(23)			2.95	−1.61
H(24)			2.95	−0.85
H(25)			1.28	−0.80
H(26)	−0.5–1.5	−0.5–1.5	1.28	0.88
H(27)			2.95	−0.41
H(28)			2.95	−1.17
H(29)			1.28	1.34

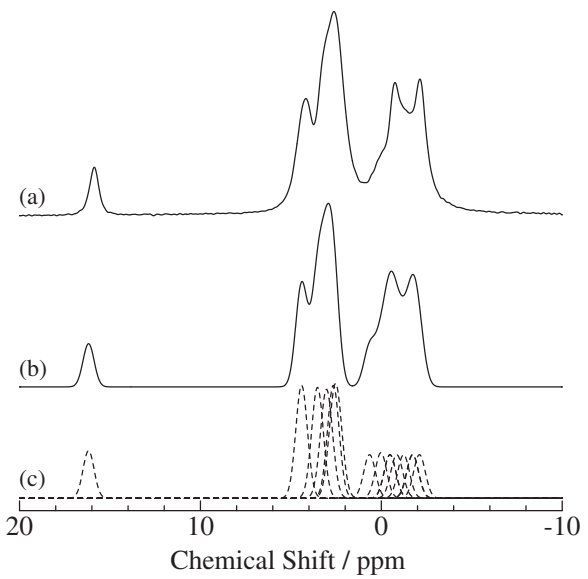

Figure 5. Spectral analysis of ^{1}H MAS NMR spectra for pyrrolidinium *p*-chlorobenzoate (PYC(H)). (a) The observed NMR line shape and (b) line envelope obtained by summing (c) each analyzing line of pyrrolidinium *p*-chlorobenzoate crystal.

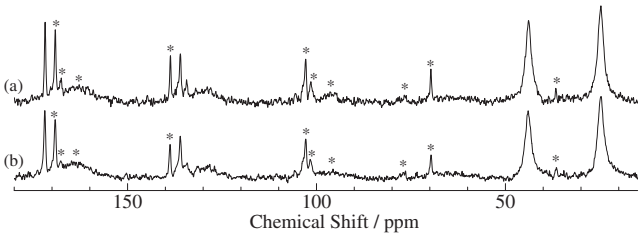

Figure 6. ^{13}C CP/MAS NMR spectra of (a) pyrrolidinium *p*-chlorobenzoate (PYC(H)) and (b) pyrrolidinium *p*-chlorobenzoate-d_2 (PYC(D)) crystals. The asterisks denote spinning-side-band peaks.

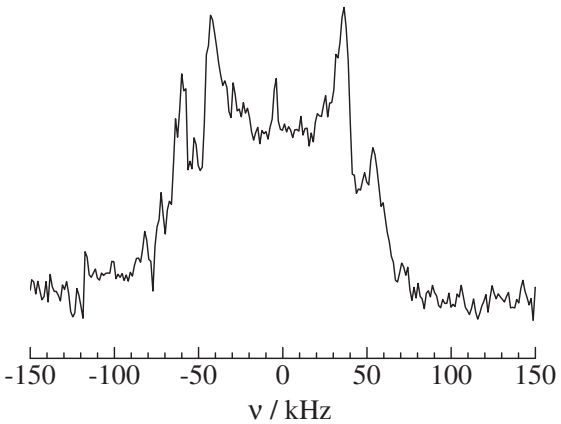

Figure 7. ^{2}H NMR spectrum of pyrrolidinium *p*-chlorobenzoate-d_2 (PYC(D)) crystals.

and CS tensor calculations with a function of B3LYP/6-311+G(3df,3pd). The obtained and assigned CS values are listed in Table 4. The obtained isotope shifts are of the same order as previously reported,[18–22] although our ^{1}H MAS NMR spectra showed significant H/D isotope changes. In addition, the observed ^{13}C signals in the PYC(H) crystals were similar to those in benzene, although ^{1}H peaks had different CS values between the crystals and those in the benzene solution. These facts suggest that ^{1}H peaks are more sensitive for detecting a small contribution from around the molecules than the ^{13}C signals.

^{2}H NMR Spectra. A ^{2}H NMR spectrum of crystalline PYC(D) obtained at room temperature is displayed in Figure 7. The obtained spectrum could be distinguished based on two lines with an asymmetric parameter (η) of 0. Employing the following relation,[30,31] quadrupole coupling constants (e^2Qqh^{-1}) of 107 and 156 kHz were estimated from each peak separation ($\Delta\nu$).

$$\Delta\nu_{\mathrm{Q}} = \frac{3}{4} e^2 Qqh^{-1} \tag{1}$$

Observing the two components of the ^{2}H NMR spectrum suggests that the D atoms in H-bond(a) and H-bond(b) have different electron envelopments, although our X-ray diffraction measurement showed an N–D length similar to that listed in Table 3. In order to assign the e^2Qqh^{-1} value that corresponds to ^{2}H atoms in H-bond(a) and H-bond(b), DFT calculations with a B3LYP/6-311+G** function were carried out. The obtained N–D length dependences of e^2Qqh^{-1} and η values

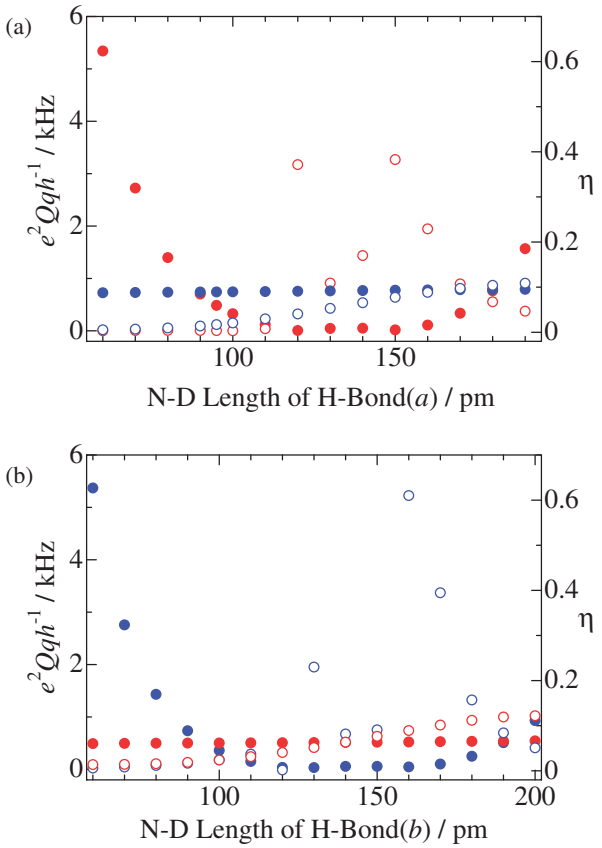

Figure 8. Estimated quadrupole coupling constant, e^2Qqh^{-1} (●) and (●) and anisotropic parameter, η (○) and (○) of ^{2}H atoms as a function of N–D length along (a) H-bond(a) and (b) H-bond(b). Here, the red and blue circles denote each parameter of the ^{2}H atoms in H-bond(a) and H-bond(b).

are shown in Figure 8. In this simulation, estimating the EFG values as a function of N–D length in H-bond(a), N–D separation in H-bond(b) was kept at 94 pm, and in contrast, calculating the N–D length dependence in H-bond(b), a constant distance of 93 pm in H-bond(a) was employed. This simulation revealed that η takes very small values around N–D lengths of 60–120 pm and large values around 120–170 pm. Our simulation showed that the principal axis of EFG is parallel to the D–N bond in a range of 60–120 pm, in contrast, the axis is perpendicular to the D–N direction in a range of 120–170 pm. Based on our estimation and the observed ^{2}H NMR spectrum with small η as shown in Figure 7, it is considerable that the short N–D separation can be obtained. This result is agreed with our X-ray diffraction data and estimated potential curves of double-minimum type described in the next section. In contrast, the calculated e^2Qqh^{-1} values disagree with the observed values for acceptable N–D lengths. This inconsistency is reasonable, because there is no consideration of the Sternheimer antishield factor (γ).[32] Introducing γ, the observed and calculated e^2Qqh^{-1} values are connected by the following relation.

$$e^2Qqh^{-1}{}_{\mathrm{obsd}} = (1-\gamma)e^2Qqh^{-1}{}_{\mathrm{calcd}} \tag{2}$$

To cancel out this empirical factor, we introduced an

$e^2Qqh^{-1}{}_{\text{obsd}}$ ratio defined by $(e^2Qqh^{-1}{}_{\text{obsd}\,a}/e^2Qqh^{-1}{}_{\text{obsd}\,b})$, where the subscripts a and b denote D atoms in H-bond(a) and H-bond(b), respectively. The $e^2Qqh^{-1}{}_{\text{obsd}}$ ratio obtained at room temperature equals 0.686 (107 kHz/156 kHz). Assuming an N–D distance of 90 pm for H-bond(a) and H-bond(b), the calculated $e^2Qqh^{-1}{}_{\text{calcd}}$ ratio defined by $(e^2Qqh^{-1}{}_{\text{calcd}\,a}/e^2Qqh^{-1}{}_{\text{calcd}\,b})$ is $0.5011/0.7370 = 0.680$. This estimated $e^2Qqh^{-1}{}_{\text{calcd}}$ ratio is similar to the observed $e^2Qqh^{-1}{}_{\text{obsd}}$ of 0.686, allowing us to assign e^2Qqh^{-1} of 156 kHz to H-bond(b) and that of 107 kHz to H-bond(a).

DFT Calculation. The potential energy calculation was carried out using a function of B3LYP/6-311+G** in the Gaussian 03w computer program.[28] In this estimation, all atomic coordinates obtained from our single-crystal X-ray measurement were employed without the H atoms contributing to hydrogen bonding along the crystallographic a- and b axis. The calculated values are shown in Figure 9a. This simulation showed four minima; the lowest energy was recorded at an N–H length of 105 pm in H-bond(a) and 98 pm in H-bond(b), the second at 155 and 98 pm, the third at 165 and 158 pm, and the forth shallow minimum at 160 and 165 pm. These results suggest that the probability of finding each H atom in H-bond(a) and H-bond(b) near the N atom is higher than that of the other side and the calculated potential curves are a double-minimum type as a function of the N–H separation. This tendency is consistent with our data obtained from the single-crystal X-ray measurements which showed that two spots with high electron density were detected near the N atom of the pyrrolidine molecule. The estimated energy differences between the potential minima were 34 and 55 kJ mol^{-1} for H-bond(a) and H-bond(b), respectively, as shown in Figures 9b and 9c.

In order to reveal the origins of the anomalous H/D isotope shift of the ^{35}Cl NQR frequency, a B3LYP/6-311+G** function was introduced into the EFG estimation. Since EFG values are in inverse proportion to the cube of the distance from a nucleus of interest to the other nuclei in the crystal, the EFG estimation was performed for 6 molecules around the p-chlorobenzoate ion. Any NQR frequency (ν_Q) of the ^{35}Cl ($I = 3/2$) nucleus is obtained by the following relations:[33,34]

$$\nu_Q = \frac{e^2Qq}{2h}\sqrt{1+\frac{\eta^2}{3}}$$
$$eq = V_{zz} \qquad \eta = \frac{|V_{xx} - V_{yy}|}{V_{zz}} \tag{3}$$

Each EFG component of V_{xx}, V_{yy}, and V_{zz} can be calculated as a function of the N–H length, and eq 3 immediately gives the N–H length dependence of the ^{35}Cl NQR frequency as shown in Figure 10. The values obtained are slightly higher than the observed frequencies in a range of acceptable N–H lengths of 70–110 pm. This inconsistency is likely due to molecular vibrations. Therefore we introduce a function C(T) which is related to the amplitude of the thermal motion:

$$\nu_{Q\ \text{obsd}} = C(T)\nu_{Q\ \text{calcd}} \tag{4}$$

Since temperature gradients of $\nu_{Q\ \text{obsd}}$ are almost the same between PYC(H) and PYC(D) over the whole measured temperature range, it is considered that the molecules in PYC(H) and PYC(D) have similar motional amplitudes at the same temperature. Therefore, the assumption of the same C(T)

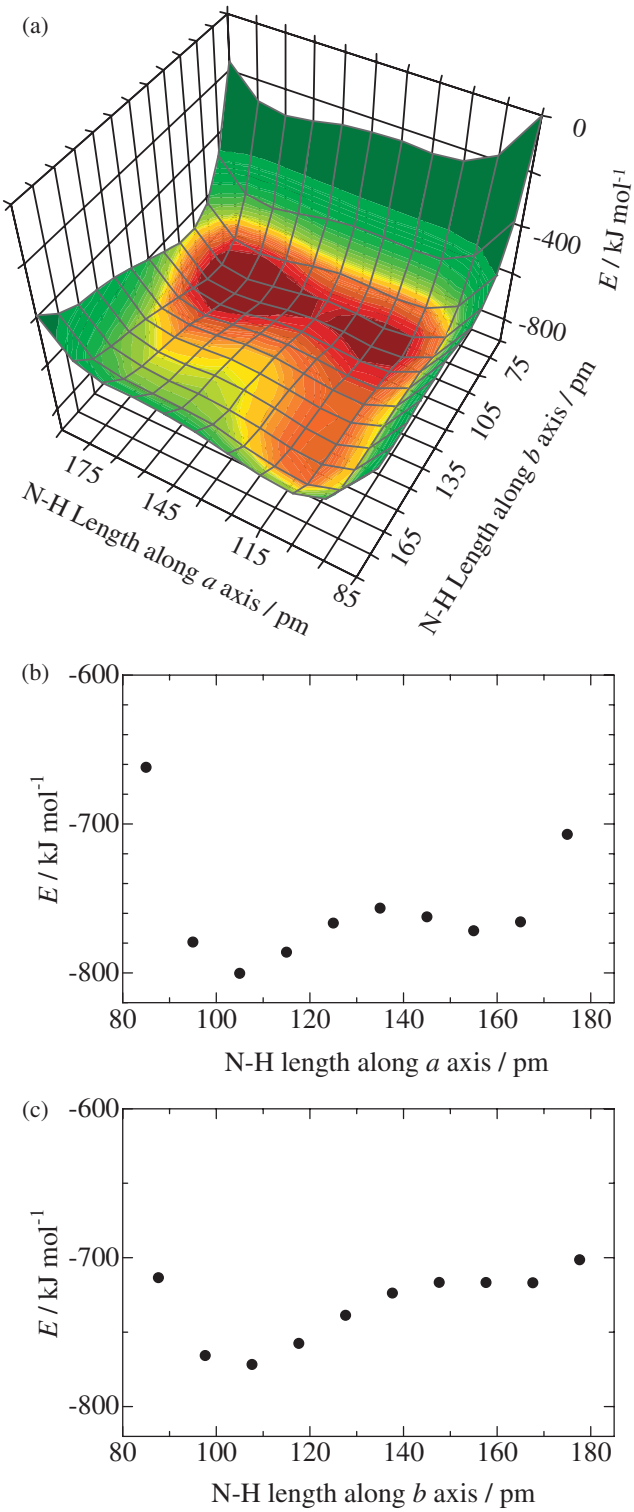

Figure 9. (a) Estimated potential-energy surface for H atoms in hydrogen bonding along crystallographic a axis and b axis. (b) Calculated N–H length dependence of the potential curve in H-bond(a) at an N–H distance of 108 pm in H-bond(b). (c) Obtained energies as a function of N–H length in H-bond(b) in the case of a constant separation of 105 pm in H-bond(a).

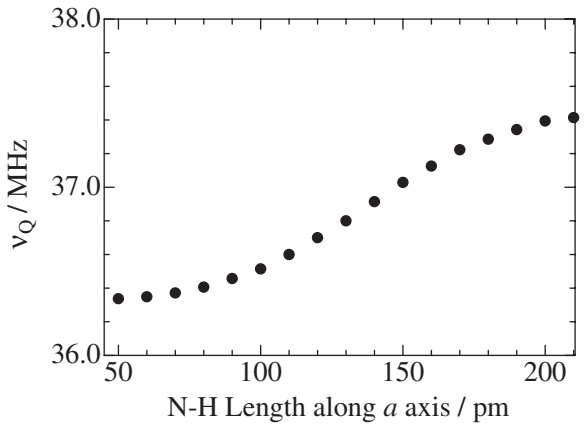

Figure 10. N–H bond length dependence of ^{35}Cl NQR frequency (ν_Q) estimated using the B3LYP/6-311+G** method.

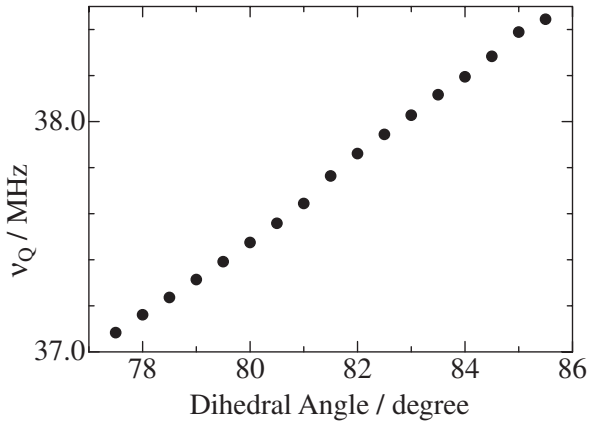

Figure 11. Calculated ^{35}Cl NQR frequency (ν_Q) dependence on the dihedral angle between benzene and piperidine ring.

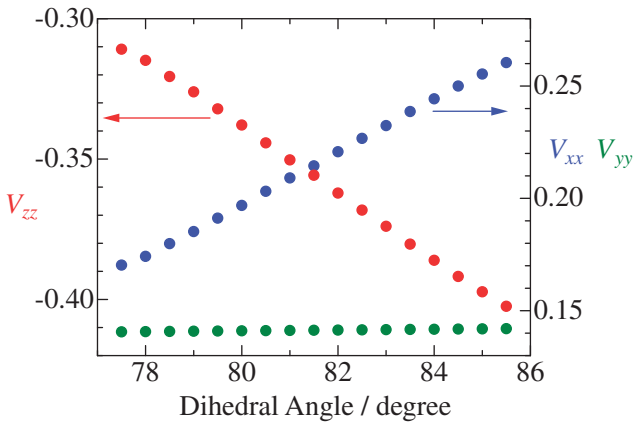

Figure 12. Dihedral angle dependence of each EFG component, V_{xx} (●), V_{yy} (●), and V_{zz} (●).

factor for PYC(H) and PYC(D) can be introduced. Based on our X-ray results of N–H length of 95 and 92 pm, respectively, for H-bond(*a*) and H-bond(*b*), a $\nu_{Q\ calcd}$ value of 36.5 MHz was immediately obtained by substitution of V_{xx}, V_{yy}, and V_{zz} into eq 3, where they were estimated by the DFT method. Since a ^{35}Cl NQR frequency of 34.30 MHz was observed for PYC(H), C(*T*) around 90 K can be arithmetically obtained to be 34.3/36.5 = 0.940. Employing this factor and the observed value of 34.00 MHz for PYC(D), a $\nu_{Q\ calcd}$ value of the deuterium substance can be estimated to be 36.2 MHz. The frequency of 34.00 MHz observed for PYC(D) corresponds to a $\nu_{Q\ calcd}$ of 36.2 MHz. To satisfy this estimated frequency of PYC(D), unacceptable N–H lengths $\ll$ 50 pm must be introduced for H-bond(*a*) and H-bond(*b*). Therefore, other mechanisms contributing to the obtained anomalous NQR frequency need to be proposed. Our single-crystal X-ray data showed another isotope change in the molecular arrangements; the dihedral angle between the benzene and pyrrolidine ring was changed by 1.1(2)° upon deuteration. The angle dependence of the calculated ^{35}Cl NQR frequency is shown in Figure 11. In this simulation, the N–H distances of 95 and 92 pm in H-bond(*a*) and H-bond(*b*) were employed. Using the observed angle of PYC(H) (80.3(1)°) and PYC(D) (79.2(1)°), an NQR frequency shift of 244 kHz was obtained by the B3LYP/6-311+G** estimation. This simulated value is similar to the observed isotope shift of 300 kHz, therefore, our calculation suggests that NQR frequencies are principally determined by the dihedral angle between the benzene–pyrrolidine ring, rather than the N–H lengths. The obtained angle change of 1.1(2)° is a normal value upon deuterium substitution, however, this ordinal change contributes to the anomalous ^{35}Cl NQR frequency.

In order to illustrate the mechanism of the isotope effect on ^{35}Cl NQR frequencies, the angle dependence of each EFG component is plotted in Figure 12. The B3LYP/6-311+G** estimation showed that the principle axis (*z* axis) of EFG is parallel to the direction of the Cl–C bond and the *x* axis is perpendicular to the benzene ring, while the *y* axis is perpendicular to the other axes; V_{zz} and V_{xx} components contain information about σ- and π-electrons on the Cl atom, respectively. Our simulation revealed that V_{yy} values were almost independent of the dihedral angle; in contrast, V_{zz} and V_{xx} values depend on the dihedral angle. Therefore, it can be concluded that not only the π-electrons but also the σ-electrons modified by the slight change in the dihedral angle of the benzene–pyrrolidine ring result in an anomalous ^{35}Cl NQR frequency shift. Our single-crystal X-ray diffraction measurement showed that the nearest atom from the Cl atom is H(28) in pyrrolidinium ion and the second is H(10) in *p*-chlorobenzoate ion, and the distances of Cl···H(28) and Cl···H(21) were, respectively, changed by 10 and 3 pm upon deuteration as shown in Table 2. It can be roughly estimated that H(28) and H(21) atoms are placed on *z* and *x* direction from the Cl atom, respectively. Therefore it is considerable that the dihedral angle change results in Cl···H intermolecular distances changes and effect to ^{35}Cl NQR frequency shifts.

To reveal the dihedral angle and N–H length dependences of the ^{1}H CS values, a B3LYP/6-311+G(3df,3pd) method was introduced into one couple of pyrrolidine and *p*-chlorobenzene molecules, and a PM3 function was applied on 4 molecules around them. In this calculation, the atomic coordinates based on our crystallographic data, as listed in Table 2, were employed. In order to obtain simulated CS values of the ^{1}H and ^{13}C nucleus, shielding-tensor calculation of tetramethylsilane (TMS) was carried out by the same function of B3LYP/6-311+G(3df,3pd). Subtracting the estimated shielding tensors

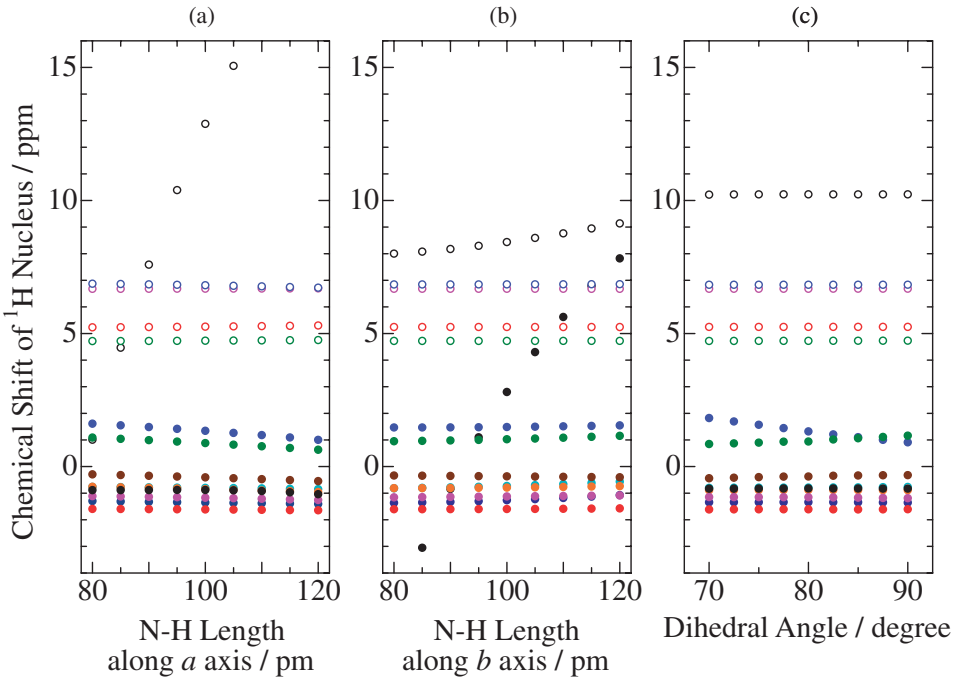

Figure 13. ^{1}H NMR chemical shift dependence on N–H bond distance along (a) crystallographic *a* axis and (b) *b* axis, and (c) on dihedral angle between benzene and pyrrolidine ring estimated by B3LYP/6-311+G(3df,3pd). H(16) (○), H(17) (●), H(18) (○), H(19) (○), H(20) (○), H(21) (○), H(22) (●), H(23) (●), H(24) (●), H(25) (●), H(26) (●), H(27) (●), H(28) (●), H(29) (●).

from those of TMS, CS values were immediately obtained. Simulated CS values, depending on the dihedral angle and on N–H separations, are shown in Figure 13. Since our calculated CS values listed in Table 4 were inconsistent with the observed ones in the range of acceptable dihedral angles and N–H separations, some basis functions of 6-31+G**, 6-311+G**, cc-pVDZ, cc-pVTZ, and AUG-cc-pVDZ were introduced into the above model. The obtained results are shown in Figure 14. All the methods employed showed inconsistent CS values with the detected ones. This fact is considerable that the used model and/or functions were insufficient with CS estimation. However, calculation with more molecules and/or with a high level method (e.g., MP2, MP4), instead of the DFT method and/or B3LYP/6-31+G** in place of the PM3 function, could not be worked out on our computer power, therefore, we discuss the CS difference with a parameter of the dihedral angle and the N–H distance rather than numerical CS values. Before discussing the CS dependence of the angle and the lengths, we describe the assignment of each peak. Our simulation showed that the CS values of H(26) and H(29) are larger than H(22) and H(25), although H(26) and H(22), and H(29) and H(25) are, respectively, bonded on the same C atom and little frequency differences of H(23) − H(27) and H(24) − H(28) are estimated. This result is considerable to effects of H-bond(*b*), because H(26) and H(29) atoms are closer to H(17) in H-bond(*b*) than H(22) and H(25). Figures 13 and 14 indicate that CS values of H(26) and H(29) atoms are most sensitive to the dihedral angle and the N–H distances without those of H(16) and H(17) which are substituted by ^{2}H atoms. Since the ^{1}H MAS NMR lines obtained around 0 ppm are significantly changed upon deuteration, our simulation results are consistent with the observed spectrum. Our line simulation suggests that the signal around

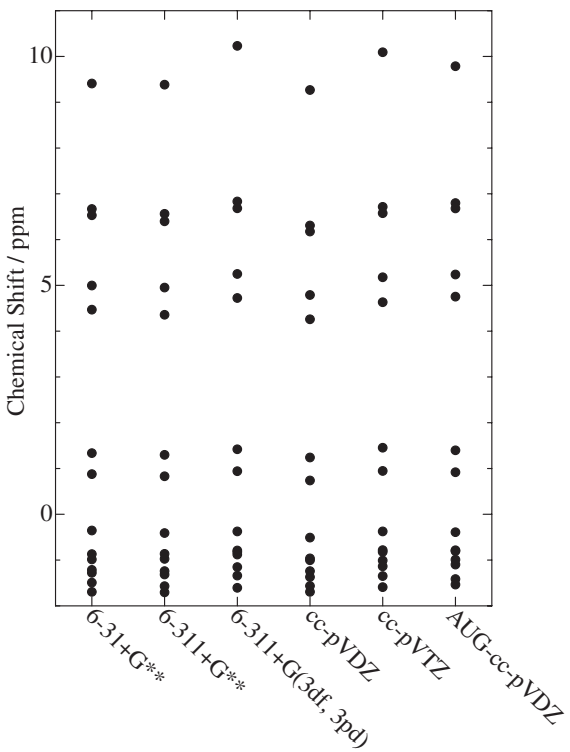

Figure 14. Simulated ^{1}H NMR chemical shift dependence on the basis function of 6-31+G**, 6-311+G**, 6-311+G(3df,3pd), cc-pVDZ, cc-pVTZ, and AUG-cc-pVDZ.

0 ppm should be composed of additional components; these could not however be uniquely determined. Our estimation showed that CS values of H(26) and H(29) atoms strongly

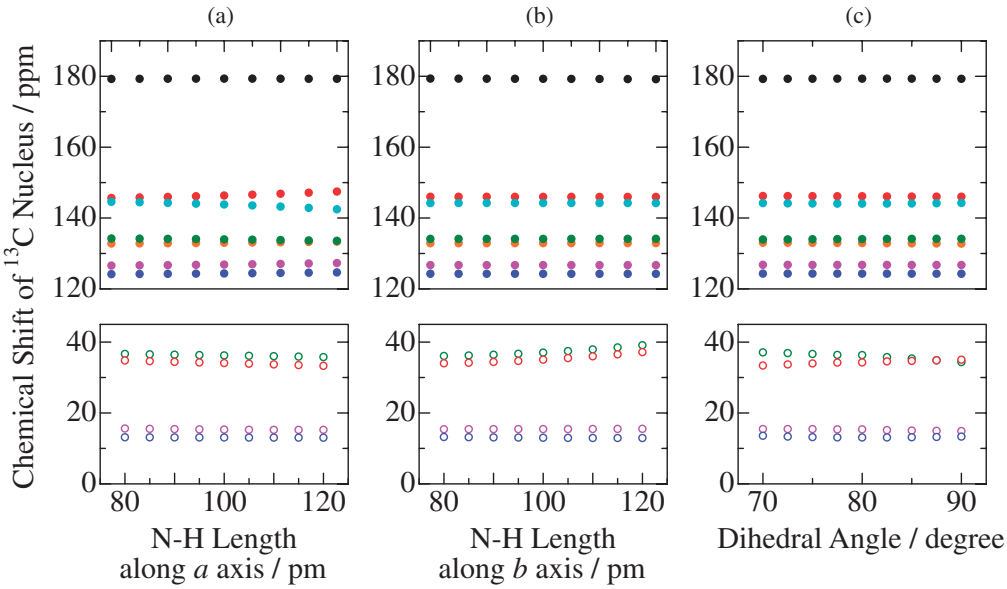

Figure 15. ^{13}C NMR chemical shift dependence on N–H bond distance along (a) crystallographic *a* axis, (b) *b* axis, and (c) on the dihedral angle between benzene and pyrrolidine ring estimated by B3LYP/6-311+G(3df,3pd). C(1) (●), C(2) (●), C(3) (●), C(4) (●), C(5) (●), C(6) (●), C(7) (●), C(8) (○), C(9) (○), C(10) (○), C(11) (○).

depend on the dihedral angle compared to the N–H distances in a range of acceptable angle and length. This fact can be explained on the basis of the dihedral angle change: the smaller dihedral angle results in the shorter distance between these H atoms and π electrons on the carboxyl group of the *p*-chlorobenzoate ion which is stacked with the pyrrolidinium ion along the crystallographic *b* axis.

Simulated CS values of ^{13}C atoms rarely depend on both the N–H lengths and the dihedral angle as shown in Figure 15, where the same function of B3LYP/6-311+G(3df,3pd) and model were employed as those of ^{1}H atoms. This result is consistent with the fact that the observed ^{13}C CP/MAS NMR peaks showed small shifts by deuteration as indicated in Figure 6.

Conclusion

Anomalous H/D isotope effects were recorded for the ^{35}Cl NQR frequency of pyrrolidinium *p*-chlorobenzoate crystals. A ^{35}Cl NQR frequency of about 280 kHz was observed by deuterium substitution of hydrogen atoms in N–H···O type H-bonds. The results of ^{1}H T_1 measurements revealed that anomalous H/D isotope effects on ^{35}Cl NQR frequencies are due to static changes rather than dynamic ones. Our single-crystal X-ray diffraction measurement results for PYC(H) and PYC(D) showed that the dihedral angle between the benzene and pyrrolidine rings changed from 80.3 to 79.2° and the N–H lengths become shorter upon deuteration. DFT calculation employing the B3LYP/6-311++G** function demonstrated that the dihedral angle change of 1.1° contributes to anomalous NQR frequency changes, frequently detected in some crystals by deuterium substitutions, rather than the N–H distance. In addition, our simulation revealed that EFG components along σ- and π-orbitals on the Cl atom of the pyrrolidinium ion are sensitive to the dihedral angle of the present crystal.

^{1}H MAS NMR measurements recorded significant envelop changes upon deuteration. Our CS simulation with the B3LYP/6-311+G(3df,3pd) method as a function of the dihedral angle and N–H lengths showed that the former also affects chemical shifts of ^{1}H atoms. In addition, we were able to demonstrate that ^{1}H MAS NMR measurements are a good tool for studying small changes in electron states compared to the ^{13}C CP/MAS NMR method, because the ^{1}H MAS NMR spectra were changed by deuterium substitution in the crystal and displayed different CS values of the material in benzene solution.

The authors are grateful to Prof. R. Ikeda of the University of Tsukuba for the use of the MSL-300 and SXP spectrometers, to Dr. M. Yamauchi of the University of Tsukuba for supporting T_1 measurements, and to Dr. S. Kita of Yokohama City University for useful instructions about DFT calculations. This work was partly supported by a Grant in Support of Promotion of Research at Yokohama City University.

References

1 G. A. Jeffrey, *An Introduction to Hydrogen Bonding*, Oxford University Press, New York, **1997**.
2 S. Scheiner, *Hydrogen Bonding*, Oxford University Press, New York, **1997**.
3 Y. Marechal, *The Hydrogen Bond and the Water Molecule*, Elsevier, Amsterdam, **2007**.
4 E. Matsushita, T. Matsubara, *Prog. Theor. Phys.* **1982**, *67*, 1.
5 R. Blinc, M. Mali, Z. Trontelj, *Phys. Lett. A* **1967**, *25*, 289.
6 W. Pies, A. Weiss, *Adv. Nucl. Quadrupole Reson.* **1974**, *7*, 57.
7 R. J. Lynch, T. C. Waddington, T. A. O'Shea, J. A. S. Smith, *J. Chem. Soc., Faraday Trans. 2* **1976**, *72*, 1980.
8 D. Borchers, A. Weiss, *Ber. Bunsen-Ges.* **1986**, *90*, 718.
9 W. M. Shirley, *Spectrochim. Acta, Part A* **1987**, *43*, 565.

10 A. Sasane, H. Shinohara, Y. Mori, Y. Kume, T. Asaji, D. Nakamura, *Z. Naturforsch., A: Phys. Sci.* **1987**, *42*, 611.
11 M. Maćkowiak, P. Koziol, *Phys. Status Solidi A* **1988**, *108*, 739.
12 J. Kalenik, I. Majerz, Z. Malarski, L. Sobczyk, *Chem. Phys. Lett.* **1990**, *165*, 15.
13 K. Horiuchi, *J. Chem. Soc., Faraday Trans.* **1993**, *89*, 3359.
14 M. Zdanowska-Fraczek, *J. Mol. Struct.* **1994**, *321*, 53.
15 M. Zdanowska-Fraczek, *Ber. Bunsen-Ges.* **1998**, *102*, 340.
16 H. Honda, *Z. Naturforsch., A: Phys. Sci.* **2003**, *58*, 623.
17 R. Nakano, H. Honda, T. Kimura, E. Nakata, S. Takamizawa, S. Noro, S. Ishimaru, *Hyperfine Interact.* **2008**, *181*, 59.
18 P. E. Hansen, S. Bolvig, K. Wozniak, *J. Mol. Struct.* **2005**, *749*, 155.
19 P. E. Hansen, *J. Labelled Compd. Radiopharm.* **2007**, *50*, 967.
20 T. T. Nguyen, T. N. Le, F. Duus, B. K. V. Hansen, P. E. Hansen, *Magn. Reson. Chem.* **2007**, *45*, 245.
21 J. P. Hofmann, F. Duus, A. D. Bond, P. E. Hansen, *J. Mol. Struct.* **2006**, *790*, 80.
22 P. E. Hansen, F. S. Kamounah, B. K. V. Hansen, J. Spanget-Larsen, *Magn. Reson. Chem.* **2007**, *45*, 106.
23 S. Kashino, Y. Sumida, M. Haisa, *Acta Crystallogr., Sect. B* **1972**, *28*, 1374.
24 S. Kashino, S. Kataoka, M. Haisa, *Bull. Chem. Soc. Jpn.* **1978**, *51*, 1717.
25 G. Metz, X. Wu, S. O. Smith, *J. Magn. Reson. A* **1994**, *110*, 219.
26 G. M. Sheldrick, *SADABS, Program for Area Detector Adsorption Correction*, Institute for Inorganic Chemistry, University of Göttingen, Germany, **1996**.
27 G. M. Sheldrick, *Acta Crystallogr., Sect. A* **2008**, *64*, 112.
28 M. J. Frisch, G. W. Trucks, H. B. Schlegel, G. E. Scuseria, M. A. Robb, J. R. Cheeseman, J. A. Montgomery, Jr., T. Vreven, K. N. Kudin, J. C. Burant, J. M. Millam, S. S. Iyengar, J. Tomasi, V. Barone, B. Mennucci, M. Cossi, G. Scalmani, N. Rega, G. A. Petersson, H. Nakatsuji, M. Hada, M. Ehara, K. Toyota, R. Fukuda, J. Hasegawa, M. Ishida, T. Nakajima, Y. Honda, O. Kitao, H. Nakai, M. Klene, X. Li, J. E. Knox, H. P. Hratchian, J. B. Cross, C. Adamo, J. Jaramillo, R. Gomperts, R. E. Stratmann, O. Yazyev, A. J. Austin, R. Cammi, C. Pomelli, J. W. Ochterski, P. Y. Ayala, K. Morokuma, G. A. Voth, P. Salvador, J. J. Dannenberg, V. G. Zakrzewski, S. Dapprich, A. D. Daniels, M. C. Strain, O. Farkas, D. K. Malick, A. D. Rabuck, K. Raghavachari, J. B. Foresman, J. V. Ortiz, Q. Cui, A. G. Baboul, S. Clifford, J. Cioslowski, B. B. Stefanov, G. Liu, A. Liashenko, P. Piskorz, I. Komaromi, R. L. Martin, D. J. Fox, T. Keith, M. A. Al-Laham, C. Y. Peng, A. Nanayakkara, M. Challacombe, P. M. W. Gill, B. Johnson, W. Chen, M. W. Wong, C. Gonzalez, J. A. Pople, *Gaussian 03 (Revision B.04)*, Gaussian, Inc., Pittsburgh PA, **2003**.
29 C. F. Macrae, I. J. Bruno, J. A. Chisholm, P. R. Edgington, P. McCabe, E. Pidcock, L. Rodriguez-Monge, R. Taylor, J. van de Streek, P. A. Wood, *J. Appl. Cryst.* **2008**, *41*, 466.
30 A. Abragam, *The Principles of Nuclear Magnetism*, Oxford University Press, London, **1961**.
31 M. H. Cohen, F. Reif, *Solid State Phys.* **1957**, *5*, 321.
32 E. A. C. Lucken, *Nuclear Quadrupole Coupling Constants*, Academic Press, London **1969**, Chapt. 5.
33 H. Bayer, *Z. Phys. A: Hadrons Nucl.* **1951**, *130*, 227.
34 T. Kushida, *J. Sci. Hiroshima Univ., Ser. A* **1955**, *19*, 327.